 CMES, vol.30, no.1, pp.37-56, 2008

# The MLPG Mixed Collocation Method for Material Orientation and Topology Optimization of Anisotropic Solids and Structures

**Shu Li**[1] **and S. N. Atluri**[2]

**Abstract:** In this paper, a method based on a combination of an optimization of directions of orthotropy, along with topology optimization, is applied to continuum orthotropic solids with the objective of minimizing their compliance. The spatial discretization algorithm is the so called Meshless Local Petrov-Galerkin (MLPG) "mixed collocation" method for the design domain, and the material-orthotropy orientation angles and the nodal volume fractions are used as the design variables in material optimization and topology optimization, respectively. Filtering after each iteration diminishes the checkerboard effect in the topology optimization problem. The example results are provided to illustrate the effects of the orthotropic material characteristics in structural topology-optimization.

**Keyword:** orthotropy, material-axes orientation optimization, topology optimization, meshless method, MLPG, collocation, mixed method

## 1 Introduction

The use of anisotropic materials in structural design provides superior physical and mechanical properties in a wide range of engineering applications such as complex aircraft: low-mass army ground-vehicles, simple sails: high speed and light rotating disks [Spalatelu-Lazar, Léné and Turbé(2008), Khoshnood and Jalali (2008)]. Composite materials are used to design a material with properties which are impossible to be achieved by isotropic materials. It is well known that the characteristics and properties of composite structures made of orthotropic materials are directly related to the orientation of material principal axes. For complicated engineering structures with many design parameters, simple structural design is not sufficient for the desired structural performance. Topology optimization is becoming a potentially important tool for structural design. By adding material where it is required for desired performance, and by removing material where it is redundant, while keeping the volume of the structure constant, topology optimization methods transform the structural design problem into a material distribution optimization problem.

The conventional topology optimization of a structure proceeds in a sequential manner, and it simultaneously solves the equilibrium equations and optimizes the structure subjected to certain objectives and constraints [Norato, Bendsøe, Haber and Tortorelli (2007), Vemaganti and Lawrence (2005), Cisilino(2006), Wang, Lim, Khoo and Wang (2007), Zhou and Wang (2006)]. Simpler, convenient and efficient numerical methods are also mandatory, because of the intensive computation involved in topology optimization. With the potential benefits of the meshless methods, especially research in [Atluri and Zhu(1998), Atluri and Shen(2002a, 2002b), and Atluri(2004)] shows that the MLPG method is becoming the most effective numerical-analytical method for optimizing structures. In this paper, the equilibrium equations of the topology optimization problem are solved by a Meshless Local Petrov-Galerkin (MLPG) "mixed collocation" method which was presented by Atluri, Liu, and Han (2006). This meshless method avoids any numerical integration either over a local domain or over the local boundary and has inherent advantages such as the computational efficiency and the ease of implementation.

In the present work, we extend our previous work

[1] Department of Aircraft Engineering, Beijing University of Aeronautics and Astronautics, Beijing 100083, P.R. China
[2] Center for Aerospace Research & Education, University of California, Irvine, USA

[Li and Atluri (2008)] to perform topology optimization of orthotropic composite structures. This work focuses on a combination of the optimization of material-axes orientation, along with topology optimization, of orthotropic continuum solids. We deal with this problem in two stages. The first stage is based on ideas from optimization of orientation angles of an orthotropic material. The orientations of orthotropic materials are important design parameters, because they can change the structural mechanical behavior. In the "orientation-optimization" of an orthotropic material, one of the early works is due to Pedersen (1989). The objective of the optimization is to treat the compliance minimization as a measure of the material stiffness. To this end the compliance of the structure is evaluated using the Meshless Local Petrov-Galerkin (MLPG) "mixed collocation" method, the one already used by the authors for isotropic plane structures [Li and Atluri (2008)]. Finally, a topology optimization of the orthotropic composite structure, with the optimized material orientations, is performed. The methods can be easily extended to thick-section composite laminates, wherein each lamina can be modeled as an orthotropic material. *The methods that are developed in the present paper, and in Li and Atluri (2008) are germane to our overall goal of implementing multi-scale material and topology optimization strategies for maximizing the fracture and damage resistance of light weight structures subject to intense dynamic loading.*

The outline of this paper is as follows: the MLPG mixed collocation method is introduced in Section 2, where the moving least squares (MLS) approximation is briefly reviewed and the equilibrium equations for an anisotropic solid are discussed. An "optimal orientation-of-material-angles" problem of an anisotropic material is defined in Section 3. Section 4 gives the formulation for the structural topology optimization, a scheme for the Lagrange method and the filtering principle. Several examples are presented to illustrate the characteristics of topology optimization for orthotropic materials, in section 5. Finally, we summarize, discuss, and generalize the results of the paper in section 6.

## 2 MLPG Mixed Collocation Method

### 2.1 The moving least squares (MLS) approximation

The moving least squares (MLS) approximation is often chosen as the interpolation function in a meshless approximation of the trial function. The MLPG Mixed Collocation Method adopts the MLS interpolation [while other functions such as the Radial Basis Functions, MQ, etc. can also equally well be used] to approximate a function $\mathbf{u}(\mathbf{x})$ over a number of nodes randomly spread within the domain of influence. The approximated function $\mathbf{u}(\mathbf{x})$ can be written as [Atluri (2004)]

$$\mathbf{u}(\mathbf{x}) = \mathbf{p}^T(\mathbf{x})\mathbf{a}(\mathbf{x}) \tag{1}$$

where $\mathbf{p}^T(\mathbf{x})$ is a monomial basis which can be expressed as $\mathbf{p}^T(\mathbf{x}) = [1, x_1, x_2]$ for two-dimensional problems and $\mathbf{p}^T(\mathbf{x}) = [1, x_1, x_2, x_3]$ for three dimensional problems, respectively. $\mathbf{a}(\mathbf{x})$ is a vector of undetermined coefficients, which can be obtained by minimizing the weighted discrete $L_2$ norm, defined as

$$J(\mathbf{x}) = \sum_{I=1}^{m} \mathbf{w}_I(\mathbf{x}) \left[\mathbf{p}^T(\mathbf{x}_I)\,\mathbf{a}(\mathbf{x}) - \hat{u}^I\right]^2 \tag{2}$$

where $\{\mathbf{x}_I\} : (I = 1, 2, \ldots, m)$ are scattered local points (nodes) to approximate the function $\mathbf{u}(\mathbf{x})$, $\mathbf{w}_I$ are the weight functions and $\hat{u}^I$ are the fictitious nodal values. After the coefficient vector $\mathbf{a}(\mathbf{x})$ is obtained, we substitute it into Eq. (1). The function $\mathbf{u}(\mathbf{x})$ can be approximated by these fictitious nodal values, as

$$u(\mathbf{x}) = \sum_{I=1}^{m} \Psi^I(\mathbf{x})\hat{u}^I \tag{3}$$

where $\hat{u}^I$ is the virtual nodal value at node $I$, and $\Psi^I(\mathbf{x})$ is the shape function. The detailed formulations and discussions for the MLS interpolation, using the true nodal values can be found in Atluri (2004).

Generally speaking, the MLS shape function does not have the Dirac Delta property, namely

$$u^I \equiv u(\mathbf{x}^I) = \sum_{J=1}^{m} \Psi^J(\mathbf{x})\,\hat{u}^I \neq \hat{u}^I \tag{4}$$

However, with the mapping relationship between the virtual and true nodal values [Eq. (4)], it is straightforward to establish the trial functions in the true nodal-values space as

$$u(\mathbf{x}) = \sum_{I=1}^{m} \Phi^I(\mathbf{x}) u^I \tag{5}$$

### 2.2 Equilibrium equations

We consider a linear elastic body $\Omega$ undergoing infinitesimal deformations. The equilibrium equation can be expressed as

$$\nabla \cdot \boldsymbol{\sigma} + \mathbf{f} = \mathbf{0} \tag{6}$$

subject to the boundary conditions:

$$\begin{aligned} &\mathbf{u} = \overline{\mathbf{u}} \quad \text{on } \Gamma_u \\ &\mathbf{t} = \mathbf{n} \cdot \boldsymbol{\sigma} = \overline{\mathbf{t}} \quad \text{on } \Gamma_t \end{aligned} \tag{7}$$

In which $\boldsymbol{\sigma}$ is the stress tensor, $\nabla$ is the gradient vector, $\mathbf{f}$ is the body force vector; $\mathbf{u}$ is the displacement vector, $\mathbf{t}$ is the traction vector, and $\mathbf{n}$ is the outward unit normal to the boundary $\Gamma$.

Within the general MLPG framework [Atluri(2004)], one may choose the Dirac Delta function as the test function for the unsymmetric local weak form, and apply it to each nodal point. The momentum balance equation is enforced at the nodal points, as

$$[\nabla \cdot \boldsymbol{\sigma}]\left(\mathbf{x}^I\right) + \mathbf{f}\left(\mathbf{x}^I\right) = 0 \tag{8}$$

where $\left\{\mathbf{x}^I\right\} (I = 1, 2, \ldots, N)$ are the distributed nodes, and $N$ is the number of total distributed nodes in the solution domain. In the present mixed scheme, we interpolate the displacement vector $\mathbf{u}(\mathbf{x})$ and the stress tensor $\boldsymbol{\sigma}(\mathbf{x})$ independently, using the same shape functions obtained from the MLS approximation [Eq. (3)], the displacement field $\mathbf{u}(\mathbf{x})$ and the stress field $\boldsymbol{\sigma}(\mathbf{x})$ can be represented in matrix form

$$\mathbf{u}(\mathbf{x}) = \sum_{J=1}^{m} \boldsymbol{\Phi}^J(\mathbf{x})\, \mathbf{u}^J \tag{9}$$

$$\boldsymbol{\sigma}(\mathbf{x}) = \sum_{J=1}^{m} \boldsymbol{\Phi}^J(\mathbf{x})\, \boldsymbol{\sigma}^J \tag{10}$$

Here, $\mathbf{u}^J$ and $\boldsymbol{\sigma}^J$ are the nodal displacement vector and stress vector [note that the stress tensor is now symbolically re-written as a stress-vector] at node $J$, respectively. In the case of the orthotropic linear elastic problem, the plane orthotropic constitutive relation is described by four independent material parameters and by a specified direction ($Q_{11} > Q_{22}$) as

$$\begin{bmatrix} \sigma_1 \\ \sigma_2 \\ \sigma_{12} \end{bmatrix} = \begin{bmatrix} Q_{11} & Q_{12} & 0 \\ Q_{12} & Q_{22} & 0 \\ 0 & 0 & Q_{66} \end{bmatrix} \begin{bmatrix} \varepsilon_1 \\ \varepsilon_2 \\ \varepsilon_{12} \end{bmatrix}$$

$$Q_{11} = \frac{E_1}{1 - \nu_{12}\nu_{21}}, \quad Q_{22} = \frac{E_2}{1 - \nu_{12}\nu_{21}},$$

$$Q_{66} = G_{12}, \quad Q_{12} = \nu_{12} Q_{11} = \nu_{21} Q_{22}$$

With $\mathbf{E}_1$, $\mathbf{E}_2$ the Young's modulus, $\nu_{12}, \nu_{21}$ the Poisson's ratio.

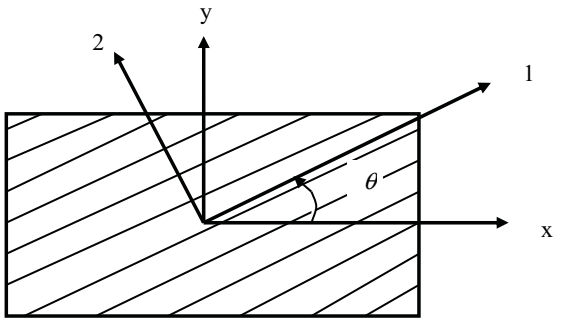


Figure 1: The orientation angle

Using a matrix expression for the rotated elastic coefficients, we can define

$$\begin{bmatrix} \sigma_1 \\ \sigma_2 \\ \sigma_{12} \end{bmatrix} = T \begin{bmatrix} \sigma_x \\ \sigma_y \\ \sigma_{xy} \end{bmatrix}$$

where the matrix T stands for the rotation matrix, $\theta$ is the orientation angle of the materials' principle direction of orthotropy. The rotation matrix $T$ can be given by

$$T = \begin{bmatrix} m^2 & n^2 & 2mn \\ n^2 & m^2 & -2mn \\ -mn & mn & \left(m^2 - n^2\right) \end{bmatrix}$$

and

$$T^{-1}=\begin{bmatrix} m^2 & n^2 & -2mn \\ n^2 & m^2 & 2mn \\ mn & -mn & \left(m^2-n^2\right) \end{bmatrix}$$

$m=\cos\theta, \quad n=\sin\theta$

The relation between the stress vector $\boldsymbol{\sigma}$ and strain vector the $\boldsymbol{\varepsilon}$ can be written as

$$\boldsymbol{\sigma}=\overline{\mathbf{Q}}\cdot\boldsymbol{\varepsilon} \tag{11}$$

Where

$$\overline{\mathbf{Q}}=\mathbf{T}^{-1}\cdot\mathbf{Q}\cdot\left(\mathbf{T}^{-1}\right)^T$$

$$\boldsymbol{\varepsilon}=\mathbf{L}^*\cdot\mathbf{u} \tag{12}$$

where, $\mathbf{L}^*$ a differential operator, for the present 2D problem.

Upon substituting the stress interpolation Eq. (10) into Eq. (8), we have

$$\sum_{J=1}^{m}\nabla\cdot\boldsymbol{\Phi}^J\left(\mathbf{x}^I\right)\cdot\boldsymbol{\sigma}^J+\mathbf{f}\left(\mathbf{x}^I\right)=0; \quad \text{for } I=1,2,\ldots,N \tag{13}$$

It clearly shows that there are no second derivatives of the shape functions for the displacements involved in the system equations, due to the independent interpolation of the stress variables. It is well known that in the meshless approximation, specifically the MLS, usually results in a very complex form of the second derivatives. The Eq. (13) has less number of equations than the number of the independent stress variables, because the nodal stress variables are more than the displacement ones. Therefore, we need to establish some more equations in addition to Eq. (11) through the stress displacement relation. The standard collocation method may be applied to enforce the stress displacement relation at each nodal point. For linear elasticity problems, this relation can be written as

$$\boldsymbol{\sigma}\left(\mathbf{x}^I\right)\overline{\mathbf{Q}}\cdot\boldsymbol{\varepsilon}\left(\mathbf{x}^I\right)=\overline{\mathbf{Q}}\cdot\mathbf{L}^*\cdot\mathbf{u}\left(\mathbf{x}^I\right) \tag{14}$$

After substituting the displacement interpolation Eq. (9) into Eq. (14), we have

$$\boldsymbol{\sigma}^J=\sum_{J=1}^{m}\overline{\mathbf{Q}}\mathbf{B}^J\left(\mathbf{x}^I\right)\mathbf{u}^J \tag{15}$$

where

$$\mathbf{B}^J\left(\mathbf{x}^I\right)=\begin{bmatrix} \Phi^J_{,x}\left(\mathbf{x}^I\right) & 0 \\ 0 & \Phi^J_{,y}\left(\mathbf{x}^I\right) \\ \Phi^J_{,y}\left(\mathbf{x}^I\right) & \Phi^J_{,x}\left(\mathbf{x}^I\right) \end{bmatrix} \tag{16}$$

$$\boldsymbol{\sigma}^J=\begin{bmatrix}\sigma^J_x & \sigma^J_y & \tau^J_{xy}\end{bmatrix}^T$$

$$\mathbf{u}^J=\begin{bmatrix}u^J_x & u^J_y\end{bmatrix}^T$$

Eq. (13) and Eq. (14) can be rewritten in the forms as follows, respectively:

$$\mathbf{K}_S\cdot\boldsymbol{\sigma}=\mathbf{f}_b \tag{17}$$

$$\boldsymbol{\sigma}=\mathbf{T}\cdot\mathbf{u} \tag{18}$$

in which $\mathbf{f}_b$ is the body force vector.

We set $\mathbf{B}_{IJ}=\mathbf{B}^J\left(\mathbf{x}^I\right)$, thus

$$\mathbf{K}_S=\begin{bmatrix} \mathbf{B}^T_{11} & \mathbf{B}^T_{12} & \cdots & \mathbf{B}^T_{1n} \\ \mathbf{B}^T_{21} & \mathbf{B}^T_{22} & \cdots & \mathbf{B}^T_{2n} \\ \vdots & \vdots & \vdots & \vdots \\ \mathbf{B}^T_{n1} & \mathbf{B}^T_{n1} & \cdots & \mathbf{B}^T_{nn} \end{bmatrix}$$

$$\mathbf{T}=\overline{\mathbf{Q}}\cdot\begin{bmatrix} \mathbf{B}_{11} & \mathbf{B}_{12} & \cdots & \mathbf{B}_{1n} \\ \mathbf{B}_{21} & \mathbf{B}_{22} & \cdots & \mathbf{B}_{2n} \\ \vdots & \vdots & \vdots & \vdots \\ \mathbf{B}_{n1} & \mathbf{B}_{n1} & \cdots & \mathbf{B}_{nn} \end{bmatrix}$$

and

$$\boldsymbol{\sigma}=\begin{bmatrix} \boldsymbol{\sigma}^1 \\ \boldsymbol{\sigma}^2 \\ \vdots \\ \boldsymbol{\sigma}^J \\ \vdots \\ \boldsymbol{\sigma}^N \end{bmatrix} \quad \mathbf{u}=\begin{bmatrix} \mathbf{u}^1 \\ \mathbf{u}^2 \\ \vdots \\ \mathbf{u}^J \\ \vdots \\ \mathbf{u}^N \end{bmatrix}$$

Let

$$\overline{\mathbf{K}}=\mathbf{K}_S\cdot\mathbf{T} \tag{19}$$

which yields the well known formulation of equilibrium equation

$$\overline{\mathbf{K}}\mathbf{u}=\mathbf{f}_b \tag{20}$$

Where

$$\overline{\mathbf{K}}_{IJ}=\sum_{K=1}^{m}\mathbf{B}^T_{IK}\overline{\mathbf{Q}}\mathbf{B}_{KJ} \tag{21}$$

It should be noted that $\mathbf{B}_{IK} = \mathbf{B}^K\left(\mathbf{x}^I\right)$ and $\mathbf{B}_{KJ} = \mathbf{B}^J\left(\mathbf{x}^K\right)$. We can write Eq.(21) as

$$\overline{\mathbf{K}}_{IJ} = \sum_{K=1}^{m} \left(\mathbf{B}^K\left(\mathbf{x}^I\right)\right)^T \hat{\mathbf{Q}} \mathbf{B}^J\left(\mathbf{x}^K\right) \tag{22}$$

Obviously, $\overline{\mathbf{K}}_{IJ}$ is not a symmetric matrix.

### 2.3 Boundary Conditions

The traction boundary conditions are enforced at each of the traction boundary nodes $K$, as:

$$\mathbf{n}^K \cdot \boldsymbol{\sigma}^K = \overline{\mathbf{t}}^K \quad \text{for } K = 1, \ldots, S \tag{23}$$

where $S$ is the number of total traction boundary nodes, the matrix $\mathbf{n}^K$ is the transformation matrix between the coordinates, as

$$\mathbf{n}^K = \begin{bmatrix} n_x^K & 0 & n_y^K \\ 0 & n_y^K & n_x^K \end{bmatrix}$$

and

$$\boldsymbol{\sigma}^K = \begin{bmatrix} \sigma_x^K & \sigma_y^K & \tau_{xy}^K \end{bmatrix}^T, \quad \overline{\mathbf{t}}^K = \begin{bmatrix} \overline{t}_x^K & \overline{t}_y^K \end{bmatrix}^T$$

Assuming $\boldsymbol{\sigma}_1$ and $\boldsymbol{\sigma}_2$ represent the known and unknown stress vectors, respectively. Hence Eq.(20) can be written as

$$\overline{\mathbf{K}}_1 \cdot \boldsymbol{\sigma}_1 + \overline{\mathbf{K}}_2 \cdot \boldsymbol{\sigma}_2 = \mathbf{f}_b \tag{24}$$

where

$$\boldsymbol{\sigma}_1 = \mathbf{T}_1 \cdot \mathbf{u} \tag{25}$$

$$\boldsymbol{\sigma}_2 = \mathbf{T}_2 \cdot \mathbf{u} \tag{26}$$

Premultiplying Eq. (23) by the penalty number $\alpha$ and the transpose of the transformation matrix $\mathbf{n}$, we obtain:

$$\alpha \mathbf{n}^T \cdot \mathbf{n} \cdot \boldsymbol{\sigma}_1 = \alpha \mathbf{n}^T \cdot \overline{\mathbf{t}} \tag{27}$$

where

$$\mathbf{n} = \begin{bmatrix} \mathbf{n}^1 & & & & & 0 \\ & \mathbf{n}^2 & & & & \\ & & \ddots & & & \\ & & & \mathbf{n}^K & & \\ & & & & \ddots & \\ 0 & & & & & \mathbf{n}^S \end{bmatrix},$$

$$\boldsymbol{\sigma}_1 = \begin{bmatrix} \boldsymbol{\sigma}^1 \\ \boldsymbol{\sigma}^2 \\ \vdots \\ \boldsymbol{\sigma}^K \\ \vdots \\ \boldsymbol{\sigma}^S \end{bmatrix} \quad \overline{\mathbf{t}} = \begin{bmatrix} \overline{\mathbf{t}}^1 \\ \overline{\mathbf{t}}^2 \\ \vdots \\ \overline{\mathbf{t}}^K \\ \vdots \\ \overline{t}^S \end{bmatrix}$$

It is easy to obtain

$$\boldsymbol{\sigma}_1 + \alpha \mathbf{n}^T \cdot \mathbf{n} \cdot \boldsymbol{\sigma}_1 = \mathbf{T}_1 \cdot \mathbf{u} + \alpha \mathbf{n}^T \cdot \overline{\mathbf{t}} \tag{28}$$

and

$$\boldsymbol{\sigma}_1 = \left(I + \alpha \mathbf{n}^T \cdot \mathbf{n}\right)^{-1} \left(\mathbf{T}_1 \cdot \mathbf{u} + \alpha \mathbf{n}^T \cdot \overline{\mathbf{t}}\right) \tag{29}$$

where I is unit matrix.

Let

$$\mathbf{R} = \left(I + \alpha \mathbf{n}^T \cdot \mathbf{n}\right)^{-1} \tag{30}$$

then

$$\boldsymbol{\sigma}_1 = \mathbf{R} \cdot \mathbf{T} \cdot_1 \mathbf{u} + \alpha \mathbf{R} \cdot \mathbf{n}^T \cdot \overline{\mathbf{t}} \tag{31}$$

By substituting Eq. (31) into Eq.(24), we can obtain a discretized system which is expressed as

$$\mathbf{K} \cdot \mathbf{u} = \mathbf{f} \tag{32}$$

where

$$\begin{aligned} \mathbf{K} &= \overline{\mathbf{K}}_1 \cdot \mathbf{R} \cdot \mathbf{T}_1 + \overline{\mathbf{K}}_2 \cdot \mathbf{T}_2 \\ \mathbf{f} &= \mathbf{f}_b - \alpha \overline{\mathbf{K}}_1 \cdot \mathbf{R} \cdot \mathbf{n}^T \cdot \overline{\mathbf{t}} \end{aligned} \tag{33}$$

## 3 Optimal orientation of material axes

We consider the problem of optimal orientation of material axes in two different problems. In the first problem, the design domain consists of an orthotropic material with a fixed orientation angle. In the second problem, the orientation angles are functions of the spatial coordinates in the design domain. The orientation optimization problem is to search for the minimization of total compliance of orthotropic material structures. The design variable is the orientation of material axes. The mean compliance is the function to be minimized with respect to the variations of the orientation angles. Here, 'compliance' is defined as the product of the external loads and the corresponding displacements.

### 3.1 The fixed orientation angle case

According to Eq.(32), the objective function (the mean compliance of a structure) is formulated as follows:

$$C(\theta) = \mathbf{f}^T \cdot \mathbf{u} \tag{34}$$

where $\mathbf{u}$ is the global displacement vector, and $\mathbf{f}$ is the prescribed force vector. Considering $C(\theta)$ as a scalar function, the above expression can also be written, for linear response, as:

$$C(\theta) = \mathbf{u}^T \mathbf{K}^T \mathbf{u} = \mathbf{u}^T \mathbf{K} \mathbf{u} \tag{35}$$

If we set $\mathbf{K}^T \mathbf{u} = \mathbf{f}'$, Eq.(35) means that the both systems of $\mathbf{K}\mathbf{u} = \mathbf{f}$ and $\mathbf{K}^T \mathbf{u} = \mathbf{f}'$ have the same compliance value under the same deformation condition.

The orientation optimization problem is treated as an unconstrained optimization problem. The mathematical statement of the orientation optimization problem is as follows:

$$\min_{\theta} C(\theta) \tag{36}$$

The optimization problem is solved using a sequential quadratic programming algorithm. This algorithm requires the sensitivity derivatives of the objective function with respect to the design variables to determine the optimal orientation of extreme compliance.

For the single orientation angle case, the orientation optimization problem only has a design variable $\theta$. We now differentiate Eq. (36) with respect to $\theta$:

$$\begin{aligned} \frac{dC(\theta)}{d\theta} &= \frac{d\mathbf{u}^T}{d\theta}\mathbf{K}\mathbf{u} + \mathbf{u}^T \frac{d\mathbf{K}}{d\theta}\mathbf{u} + \mathbf{u}^T \mathbf{K}\frac{d\mathbf{u}}{d\theta} \\ &= \mathbf{u}^T \frac{d\mathbf{K}}{d\theta}\mathbf{u} + \mathbf{u}^T \left(\mathbf{K} + \mathbf{K}^T\right) \frac{d\mathbf{u}}{d\theta} \end{aligned} \tag{37}$$

Using the fact that applied forces are design-independent of $\mathbf{K}\mathbf{u} = \mathbf{f}$ and $\mathbf{K}^T \mathbf{u} = \mathbf{f}'$, we have

$$\mathbf{K}\frac{d\mathbf{u}}{d\theta} = -\frac{d\mathbf{K}}{d\theta}\mathbf{u}$$

$$\mathbf{K}^T \frac{d\mathbf{u}}{d\theta} = -\frac{d\mathbf{K}^T}{d\theta}\mathbf{u}$$

Finally, the sensitivity derivatives of the compliance function is given by

$$\frac{dC(\theta)}{d\theta} = -\mathbf{u}^T \frac{d\mathbf{K}^T}{d\theta}\mathbf{u} \tag{38}$$

### 3.2 The distributed angles case

When the material-orientation angles are functions of spatial coordinates at discrete locations, the orientation optimization problem is a multi-variable $\theta = (\theta_1, \theta_2, \cdots, \theta_n)$ design problem. The orientation optimization problem is stated as:

$$\min_{\theta_i} C(\theta_i)$$

Eq.(38) can be extended to multiple variable cases as follows,

$$\frac{\partial C(\theta)}{\partial \theta_i} = -\mathbf{u}^T \frac{\partial \mathbf{K}^T}{\partial \theta_i}\mathbf{u} \tag{39}$$

A sequential quadratic programming algorithm is also used to solve the optimal design problem.

## 4 Topology optimization problem

### 4.1 General topology optimization

Topology-optimization implies the optimal distribution of material in a structure, so as to minimize its compliance, subject to the specified constraints of the total material to be used. According to Eq.(32), the mean compliance of a structure is formulated as follows:

$$C = \mathbf{f}^T \cdot \mathbf{u}$$

where $\mathbf{u}$ is the global displacement vector, $\mathbf{f}$ is the force vector. Also, the above expression can also be written, for linear response, as:

$$C = \mathbf{u}^T \mathbf{K} \mathbf{u} \tag{40}$$

In this paper, Eq.(40) is formed by using the MLPG Mixed Collocation Method. The design domain $\Omega$ (Fig.1) is partitioned into randomly distributed N nodes which have no connectivity in the form of a mesh. For an arbitrary node $i$, if the number of nodes around point $i$ which influence

the trial function at node $i$ is $r$, a sub-system consists of these $r$ nodes. In this sub-system, we have

$$\mathbf{k}_i \mathbf{u}_i = \mathrm{f}_i \tag{41}$$

where $\mathbf{u}_i$ is the displacement vector and $\mathbf{k}_i$ is the "stiffness" matrix constructed in the same way as Eq.(19). The MLPG form of Eq.(40) becomes

$$C = \sum_{i=1}^{N} \mathbf{u}_i^T \mathbf{k}_i \mathbf{u}_i \tag{42}$$

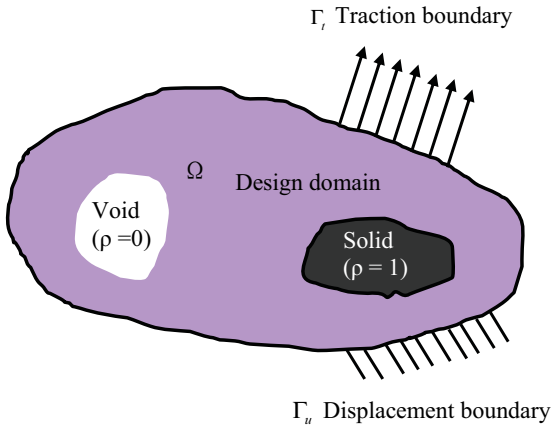


Figure 2: Topology optimization design domain

If we consider the nodal volume fractions $\rho_i$ as the design variables, then the topology optimization problem for minimizing the compliance can thus be stated, with the volume constraint $V^*$ as follows:

$$\begin{aligned} &\min_{\rho} C(\boldsymbol{\rho}) = \mathbf{u}^T \mathbf{K}\mathbf{u} = \sum_{i=1}^{N} \mathbf{u}_i^T \mathbf{k}_i \mathbf{u}_i \\ &\text{s.t.} \quad V(\boldsymbol{\rho}) = \sum_{i=1}^{N} \rho_i V_i = V^* \\ &\qquad \mathbf{K}\mathbf{u} = \mathbf{f} \\ &\qquad 0 < \rho_{\min} \le \rho_i \le 1 \end{aligned} \tag{43}$$

where $\boldsymbol{\rho}$, the vector consisting of design variable $\rho_i$ , $\rho_{\min}$, is the vector of minimum allowable relative volume fractions (non-zero to avoid singularity), $N$ is the number of nodes to discretize the design domain, and $V^*$ is the prescribed volume. $V(\rho)$ is the total volume of material.

Setting $\rho_{\min}$ to a small but positive value keeps the "stiffness" matrix $\mathbf{k}_i$ from becoming singular. The artificial variable $\rho_i$ is considered as an indicator of the local material volume $V_i$. The final material volume $V^*$ is linearly related to the design variables.

The Solid Isotropic Material with Penalization (SIMP) model leads to a common and efficient called power-law approach. To avoid intermediate volume fraction values $\rho_i$ (between 0 and 1), a SIMP-like model (Solid Isotropic Microstructure with Penalty) is adopted in the proposed topology optimization method. In this SIMP-like model, the penalized "stiffness" matrix $\mathbf{k}_i$ is given by

$$\mathbf{k}_i = (\rho_i)^p \mathbf{k}_i^0 \tag{44}$$

$\mathbf{k}_i^0$ is the initial value of the matrix $\mathbf{k}_i$, $p$ is the penalization power (typically $p$ = 3). Fig.2 displays the relative "stiffness" ratio vs. volume fraction values $\rho_i$, for different values of the penalization power $p$.

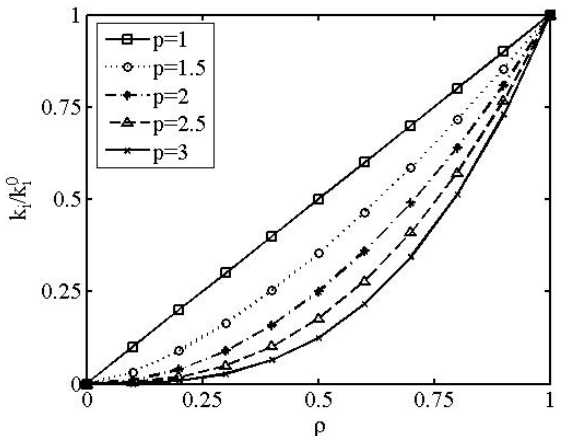


Figure 3: SIMP-like model for different values of the penalization power $p$

The MLPG Mixed Collocation Method for topology optimization problem requires the computation of the sensitivity derivatives of the compliance with respect to the design variables. The sensitivities of the compliance respect to design variable $\rho_i$ can be derived from the expression of Eq.(40) in the same manner as Eq.(39) as follows:

$$\frac{\partial C}{\partial \rho_i} = -\mathbf{u}^T \frac{\partial \mathbf{K}^T}{\partial \rho_i} \mathbf{u} \tag{45}$$

Considering the adaptation of the SIMP-like model as Eq.(44), the above expression of Eq.(45) is written as

$$\frac{\partial C}{\partial \rho_i} = -p\left(\rho_i\right)^{p-1} \mathbf{u}_i^T \left(\mathbf{k}_i^0\right)^T \mathbf{u}_i \tag{46}$$

### 4.2 The Lagrange method

The classical Lagrangian method is called as the linear Lagrangian theory in [Goh and Yang (2001)]. In the linear Lagrangian theory, the Lagrangian function is a linear combination of the objective and constraint functions for solving constrained optimization problems. Based on linear Lagrangian theory, we consider the Lagrangean associated with the constrained topology optimization problem Eq.(43)

$$L(\boldsymbol{\rho}) = C + \lambda_1 \left( \sum_{i=1}^{N} \rho_i V_i - V^* \right) + \boldsymbol{\Lambda}^T (\mathbf{Ku} - \mathbf{f}) + \sum_{i=1}^{N} \mu_1^i (\rho_{\min} - \rho_i) + \sum_{i=1}^{N} \mu_2^i (\rho_i - 1) \tag{47}$$

where $\lambda_1$ and $\mu_i$ are Lagrange multipliers for the equality and inequality constraints, respectively. $\boldsymbol{\Lambda}$ is the Lagrange multiplier vector.

To tackle this problem, the typical way of the Lagrangian method is the use the Kuhn–Tucker optimality condition which is a generalization of the first order optimality necessary conditions (FONC).

For a general classical single-objective nonlinear programming problem as:

$$\begin{aligned} &\min f(\mathbf{x}) \\ &\text{s.t.} \quad g_i(\mathbf{x}) \le 0 \quad \text{for } i = 1,2,\ldots,I \\ &\qquad h_j(\mathbf{x}) = 0 \quad \text{for } j = 1,2,\ldots,J \\ &\qquad \mathbf{x} = (x_1, x_2, \cdots, x_N) \end{aligned}$$

The Kuhn-Tucker condition is:

$$\begin{cases} \nabla f(\mathbf{x}) + \sum \mu_i \nabla g_i(\mathbf{x}) + \sum \lambda_j \nabla h_j(\mathbf{x}) = 0 \\ \qquad\qquad\qquad\qquad \text{(optimality)} \\ g_i(\mathbf{x}) \le 0 \text{ for } i = 1,2,\cdots,I \text{ (feasibility)} \\ h_j(\mathbf{x}) = 0 \text{ for } j = 1,2,\cdots,J \text{ (feasibility)} \\ \mu_i g_i(\mathbf{x}) = 0 \text{ for } i = 1,2,\cdots,I \\ \qquad \text{(complementary slackness condition)} \\ \mu_i \ge 0 \text{ for } i = 1,2,\cdots,I \text{ (non - negativity)} \\ \text{(Note: } \lambda_j \text{ is unrestricted in sign)} \end{cases}$$

The Kuhn-Tucker condition is a necessary condition for optimality in constrained minimization (or maximization) under a constraint qualification. Here, the assumption is that $\nabla g_i(\mathbf{x}^*)$ for $i$ belonging to active constraints and $\nabla h_j(\mathbf{x}^*)$ for $j$ = 1,...,$J$ are linearly independent. This is the so-called "constraint qualification".

The Kuhn-Tucker conditions not only give the necessary conditions for optimality but also provide a way of finding optimal solutions. So the Lagrange method essentially transforms a constrained problem to an unconstrained problem.

In this paper, the optimality criterion (OC) was formulated in a form suitable for incorporation in the meshless method codes. The necessary conditions for optimality can be obtained by using the Kuhn–Tucker conditions as follows:

$$\frac{\partial L}{\partial \rho_i} = 0, \quad i = 1,2,\cdots,N$$

Differentiating (47) with respect to $\rho_i$ and manipulating the terms, the Kuhn-Tucker optimality condition can be written for problems [Eq.(43)] subject to multiple constraints as follows

$$\begin{cases} \frac{\partial L}{\partial \rho_i} = \frac{\partial C}{\partial \rho_i} + \lambda_1 \frac{\partial V}{\partial \rho_i} + \boldsymbol{\Lambda}^T \frac{\partial (\mathbf{Ku})}{\partial \rho_i} - \mu_1 + \mu_2 = 0 \\ V(\boldsymbol{\rho}) \sum_{i=1}^{N} \rho_i V_i - V^* = 0 \\ \qquad\qquad \text{(the equality constraints)} \\ \mathbf{Ku} = \mathbf{f} \text{ (the equality constraints)} \\ \rho_{\min} - \rho_i \le 0 \text{ (the inequality constraints)} \\ \rho_i - 1 \le 0 \text{ (the inequality constraints)} \\ \mu_1 (\rho_{\min} - \rho_i) = 0 \\ \mu_2 (\rho_i - 1) = 0 \\ \mu_i \ge 0 \quad i = 1,2 \end{cases}$$

(48)

Note: $\lambda_1$ and $\mathbf{\Lambda}$ are unrestricted in sign, corresponding to the equality constraints. It is clear that the efficiency of the OC method is determined mainly by the number of active constraints. If $\rho_{\min} < \rho_i < 1$, the lower and upper bounds of the design variables are inactive, then we have $\mu_1 = \mu_2 = 0$. If $\rho_i = \rho_{\min}$, the lower bound of the design variables are active, then we have $\mu_1 \geq 0$, $\mu_2 = 0$. If $\rho_i = \rho_{\max}$, the upper bound of the design variables are active, then $\mu_1 = 0$, $\mu_2 \geq 0$. and (48) yields:

$$\begin{cases} \frac{\partial C}{\partial \rho_i} + \lambda_1 \frac{\partial V}{\partial \rho_i} + \mathbf{\Lambda}^T \frac{\partial (\mathbf{Ku})}{\partial \rho_i} = 0 \quad \rho_{\min} < \rho_i < 1 \\ \frac{\partial C}{\partial \rho_i} + \lambda_1 \frac{\partial V}{\partial \rho_i} + \mathbf{\Lambda}^T \frac{\partial (\mathbf{Ku})}{\partial \rho_i} \geq 0 \quad \text{if } \rho_i = \rho_{\min} \\ \frac{\partial C}{\partial \rho_i} + \lambda_1 \frac{\partial V}{\partial \rho_i} + \mathbf{\Lambda}^T \frac{\partial (\mathbf{Ku})}{\partial \rho_i} \leq 0 \quad \text{if } \rho_i = \rho_{\max} \\ V(\boldsymbol{\rho}) = \sum\limits_{i=1}^{N} \rho_i V_i - V^* = 0 \text{ (the equality constraints)} \\ \mathbf{Ku} = \mathbf{f} \text{ (the equality constraints)} \\ \mu_i \geq 0 \quad i = 1,2 \end{cases} \tag{49}$$

The above sensitivity of a node is dependent on several surrounding points. For different positions, the number of nodes around one point may different. So the sensitivity analysis is more complex and time consuming when compared with the case of element-based methods.

To derive the iterative formulation more conveniently, only the equality cases in Eq.(49) are used in the present illustration, i.e.

$$\frac{\partial C}{\partial \rho_i} + \lambda_1 \frac{\partial V}{\partial \rho_i} + \mathbf{\Lambda}^T \left( \frac{\partial \mathbf{K}}{\partial \rho_i} \mathbf{u} + \mathbf{K} \frac{\partial \mathbf{u}}{\partial \rho_i} \right) = 0$$

Utilizing the expression $\mathbf{Ku} = \mathbf{f}$, it is easy to obtain

$$\frac{\partial \mathbf{K}}{\partial \rho_i} \mathbf{u} + \mathbf{K} \frac{\partial \mathbf{u}}{\partial \rho_i} = 0$$

then

$$p(\rho_i)^{p-1} \mathbf{u}_i^T \left( \mathbf{k}_i^0 \right)^T \mathbf{u}_i + \lambda_1 V_i = 0 \tag{50}$$

Set

$$B_i = \frac{p(\rho_i)^{p-1} \mathbf{u}_i^T \left( \mathbf{k}_i^0 \right)^T \mathbf{u}_i}{\lambda_1 V_i} = 1 \tag{51}$$

Eq.(50) is regarded as an Optimally Criterion (OC) based on the discretization of the MLPG Mixed Collocation Method. Thus, we can update the design variables as follows:

$$\rho_i^{new} = \begin{cases} \max(\rho_{\min}, \rho_i - m) \\ \text{if } \rho_i B_i^{\eta} \leq \max(\rho_{\min}, \rho_i - m) \\ \\ \rho_i B_i^{\eta} \\ \text{if } \max(\rho_{\min}, \rho_i - m) < \rho_i B_i^{\eta} < \min(1, \rho_i + m) \\ \\ \min(1, \rho_i + m) \\ \text{if } \min(1, \rho_i + m) \leq \rho_i B_i^{\eta} \end{cases} \tag{52}$$

Where $m$ is the limit ([Bendsøe and Kikuchi (1988)]), which represents the maximum allowable change in the relative nodal volume fractions $\rho_i$ in the OC iteration. $\eta$ is the damping coefficient. This updating scheme was often adopted in many presented papers. The values of $m$ and $\eta$ influence the convergence of the scheme, and they are chosen by experience ([Bendsøe and Kikuchi (1988)]).

The penalty parameter $p$ is set to be 3, and the numerical damping coefficient $\eta$ is set to 0.5. The Lagrange multiplier for the volume constraint $\lambda_1$ is determined at each OC iteration using a bi-sectioning algorithm, as in the paper [Sigmund (2001)].

### *4.3 Filtering principle*

Here we describe the principle of suppressing checkerboard patterns which is a familiar problem in topology optimization when numerical stability is not guaranteed. The appearance of checkerboarding causes difficulties in interpreting and fabricating topology-optimized structural components. Sigmund (1994, 1997) developed a sensitivity filter method for preventing numerical instabilities from occurring. Filtering techniques have become quite popular in topology optimization [Wang; Lim, Khoo and Wang (2008)]. To tackle checkerboarding, a scheme similar to the filtering method is incorporated in the optimization algorithms based on the meshless discretization. In

this scheme, we modify the design sensitivity of any specific node depending on a weighted average of the node sensitivities in a connected neighborhood. The principle works by modifying the nodal sensitivities as follows

$$\frac{\widehat{\partial C}}{\partial \rho_i} = \frac{1}{\rho_i \sum_{f=1}^{m} \hat{H}_f} \sum_{f=1}^{m} \hat{H}_f \rho_f \frac{\partial C}{\partial \rho_f} \tag{53}$$

Here, the convolution operator (weight factor) is written as

$$\hat{H}_f = r_{\min} - dist\,(n,f)\,\{f \in M | dist\,(n,f) \le r_{\min}\}, \quad n = 1,\ldots,m \tag{54}$$

and the operator $dist(n, f)$ is defined as the distance between node $n$ and node $f$. The convolution operator $\hat{H}_f$ is zero outside the filter area, and decays linearly with the distance from node $f$.

## 5 Numerical examples

In this section, the examples concern two aspects of the problems with several subcases. The first aspect examines the results of the "material-axes orientation" optimization problem. The second aspect of examples examines the effect of topology optimization after finding the optimized "material-axes orientation". We present several numerical examples (cantilever and MBB-beams). All the examples are treated here as being dimensionless.

**Example 1:**

As shown in Fig. 4, the first example is that of a short cantilever beam. The material is orthotropic, with Young's moduli $E_1$ = 30, $E_2$ = 5, Poisson's ratios $\mu_{12}$ = 0·25 and the shear moduli $G_{12}$ = 2. The design domain is clamped along the left end and a concentrated vertical load P is acting at the point A, B and C respectively of the free (right) end of the beam.

The design domain Ω is discretized by the MLPG Mixed Collocation Method using uniformly distributed nodes.

**Example 2:**

The second example is that of a so-called MBB beam (Fig.7(a)) in which the right half-domain is

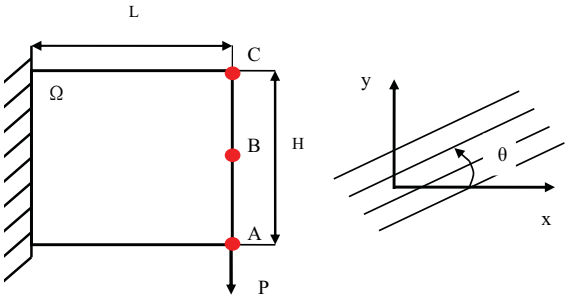


Figure 4: Cantilever beam

modeled as Fig.7(b). This is an orthotropic beam with Young's moduli $E_1$ = 30, $E_2$ = 5, Poisson's ratios $\mu_{12}$ = 0.25 and the shear moduli $G_{12}$ = 2. The design domain is discretized into 60 x 20 uniformly distributed nodes in the half-domain. The left bottom is assumed to be fixed, and the right one is assumed to be on a roller.

In the Fig.7(b), $A_t$, $B_t$, $C_t$ and $A_b$, $B_b$, $C_b$ are the 3 points at top and bottom of the MBB beam, respectively, where the concentrated vertical load P is alternatively applied. The corresponding variations of the relative compliance vs the fixed material-orientation for various locations of the point of application of the load are displayed in Fig.8 and Fig.9. When the concentrated vertical load P is applied at the middle of the top of the MBB beam, fig.10 gives the curves of the relative compliance vs the fixed material-orientation for various L/H ratio case.

Figs.5-6 in example 1, and Figs.8-10 in example 2 illustrate that the load lactation and L/H ratio influence the compliance variation significantly. From these figures, it can be seen that the compliance has different extremums, which can be searched using the optimaization method in the section 3.

**Example 3:**

The example is the same cantilever beam as in Fig.4. The optimized material-orientation vs load position with L/H=1 is shown in fig.11. The optimized material-orientation vs the L/H ratio under a concentrated vertical load P applied at the middle of the right end is shown in fig.12.

As a comparison, the considered problem was

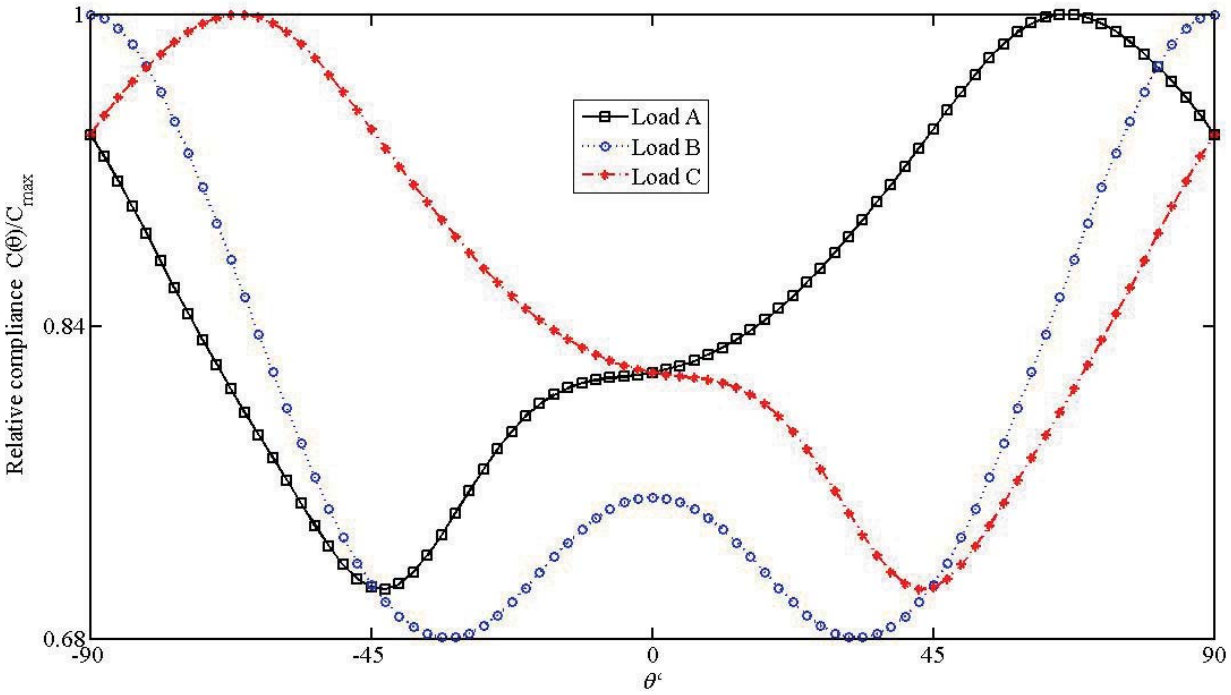


Figure 5: The relative compliance vs the fixed material-orientation for various locations of the point of application of the load (L/H=1)

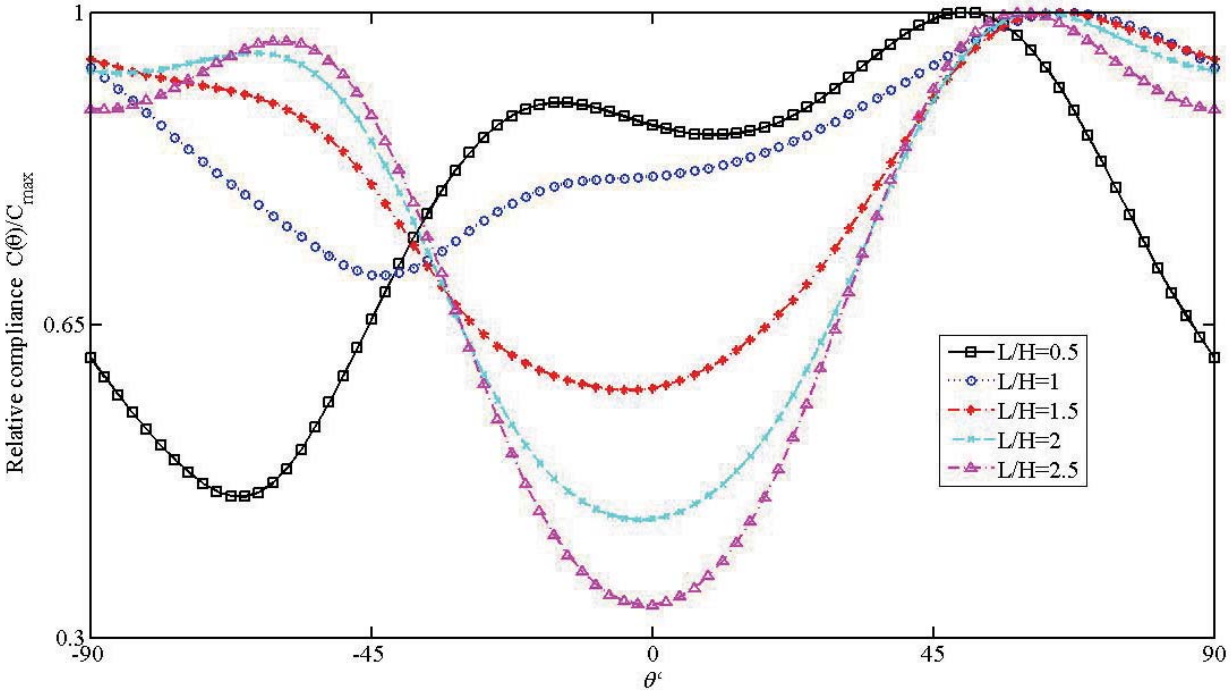


Figure 6: The relative compliance vs the fixed material-orientation for various L/H ratio cases (the load is applied at point A)

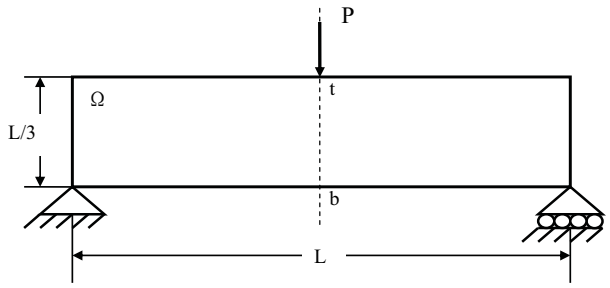


Figure 7(a): MBB beam

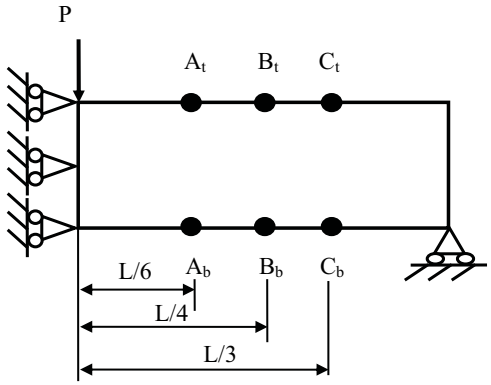


Figure 7(b): MBB beam (right half-domain)

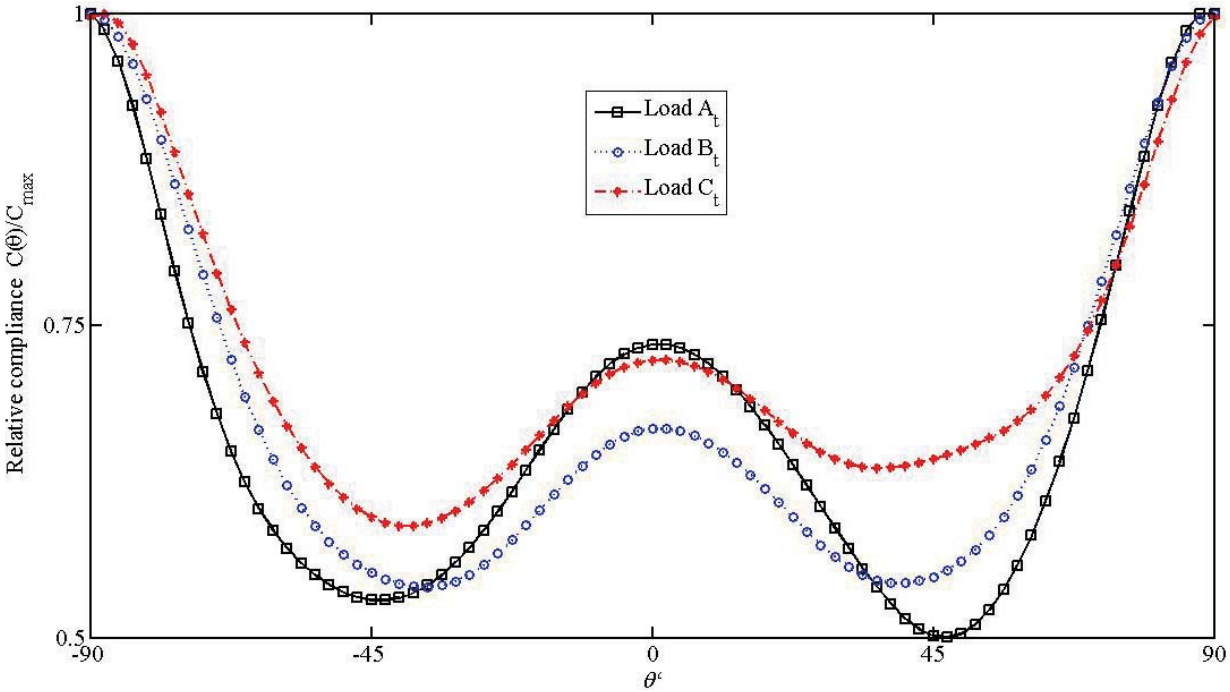


Figure 8: The relative compliance vs the fixed material-orientation for various locations of the point of application of the load (top)

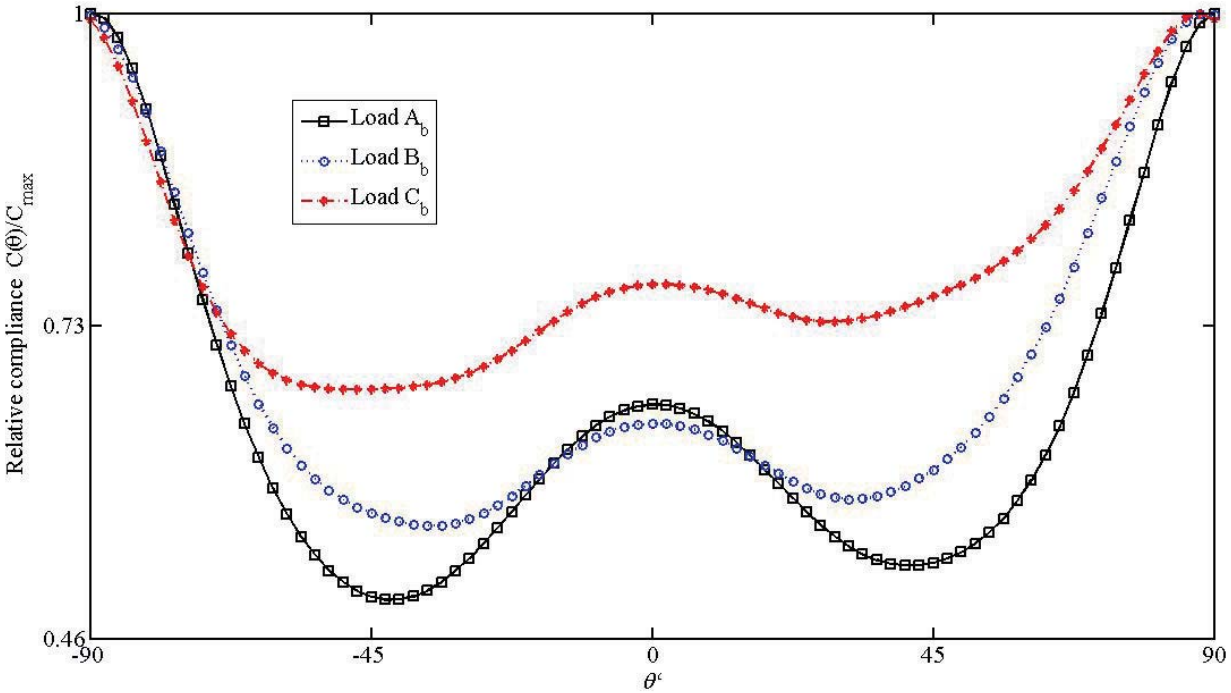


Figure 9: The relative compliance vs the fixed material-orientation for various locations of the point of application of the load (bottom)

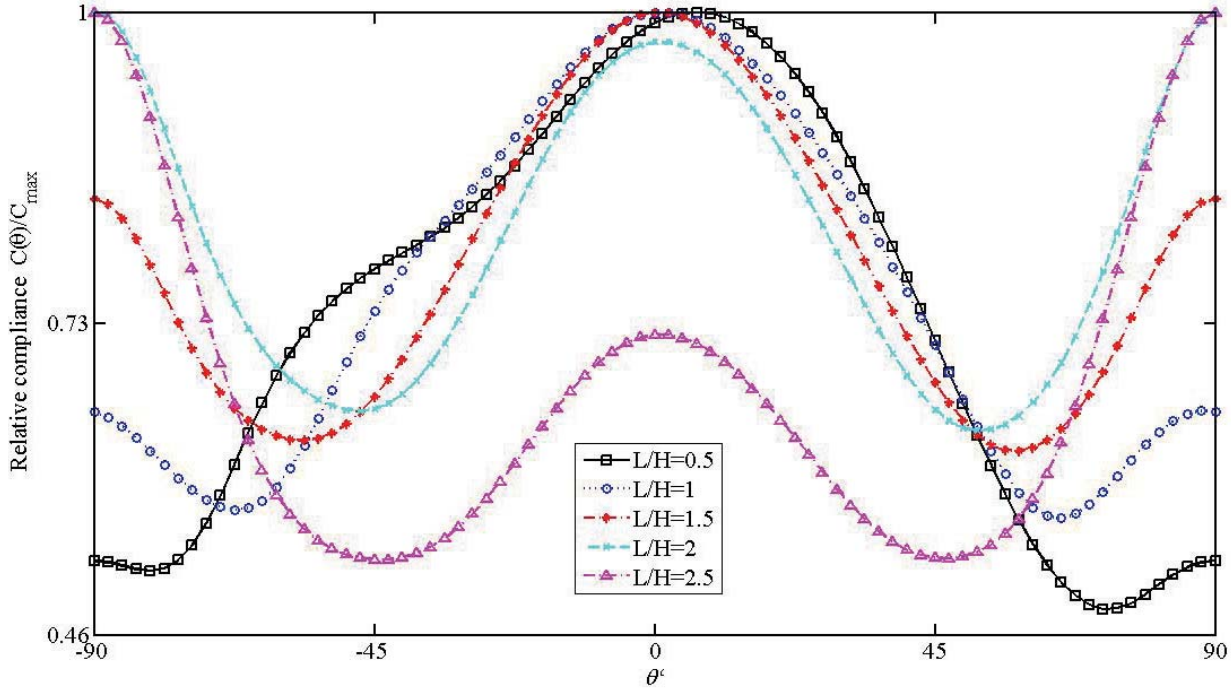


Figure 10: The relative compliance vs the fixed material-orientation for various L/H ratio cases

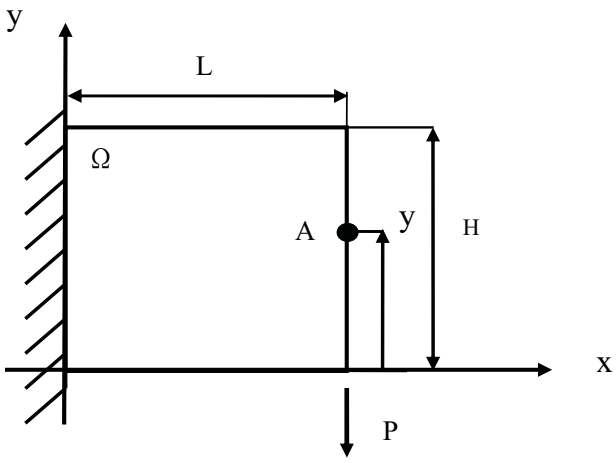


Figure 11(a): Cantilever beam model

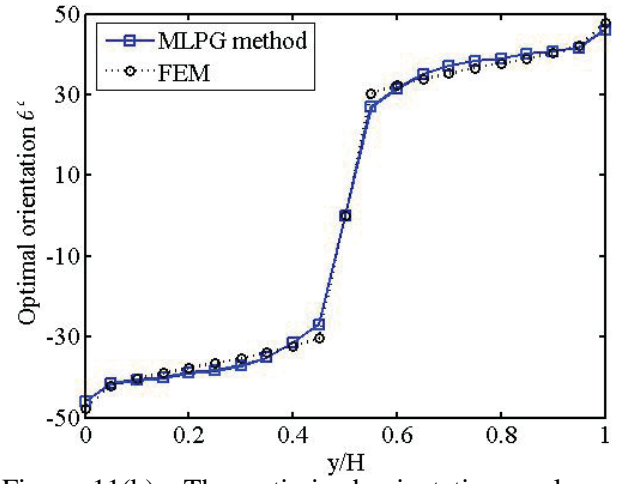


Figure 11(b): The optimized orientation angle vs load position

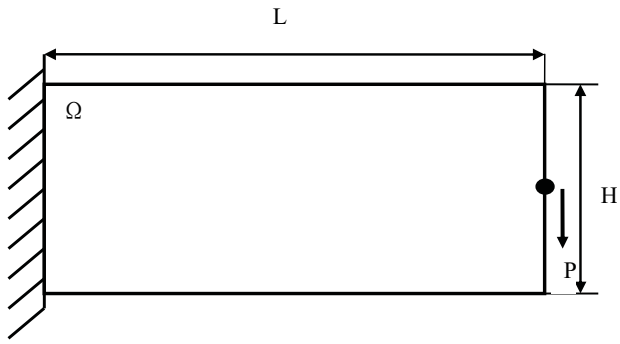


Figure 12(a): Cantilever beam model

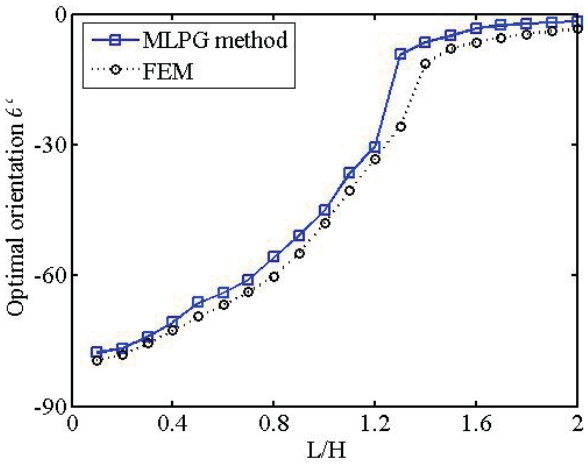


Figure 12(b): The optimized orientation angle vs the L/H ratio

also calculated by using finite element method (FEM). The results of the MLPG method are in good agreement with the solutions of the finite element method.

**Example 4:**

In this example of topology optimization, a cantilever beam as in fig. 4 is used. The design domain is discretized using 40 x 40 uniformly distributed. To compare the results of isotropic and orthotropic material cantilever beam, we choose an orthotropic material with orientation at 4 angles $\theta$ = 0˚, 45˚, 90˚ and the optimized angle, respectively.

**Example 5:**

In this example, a cantilever beam as in fig. 4 is used with L/H=1.5. The design domain is discretized using 60×40 uniformly distributed nodes. To compare the results of isotropic and orthotropic material cantilever beam, results from topology design associated with an orthotropic material oriented at $\theta$ = 0˚, ±60˚, 90˚C and the optimized angle, respectively are presented.

The results shown in Fig.13 and fig.14 display topological similarities between the isotropic material and the orthotropic one, with material axes of $\theta$ =0˚ and $\theta$ =90˚. We see that for orthotropic cases, the bending-tension coupling (i.e., $\overline{Q}_{16} = \overline{Q}_{26} = 0$) does not exist. However, the topological layouts are very different for other orthotropic material orientations since bending-tension cou-

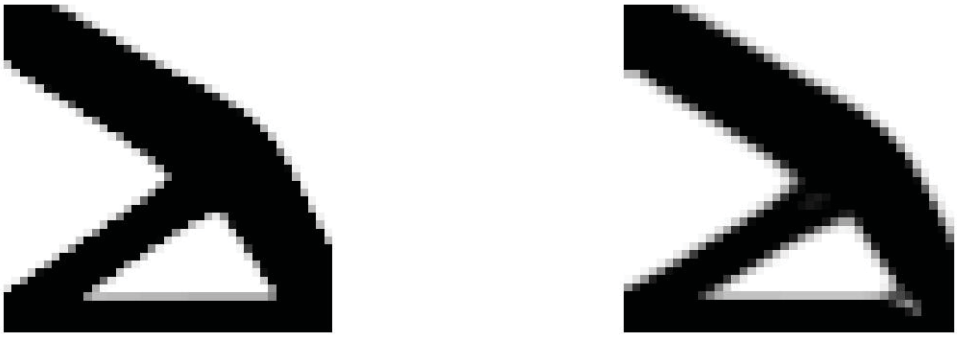

MLPG FEM

(a) Isotropic material

MLPG FEM

(b) Orthotropic material ($\theta = 0°$ )

MLPG FEM

(c) Orthotropic material ($\theta = 45°$ )

MLPG FEM

(d) Orthotropic material (θ = 90° )

MLPG FEM

(e) Orthotropic material (the optimized angle )

Figure 13: Comparison of topology optimization results

pling are significant enough to change the layouts. It is also shown that the result obtained by the MLPG method is identical to that of the finite element method. Furthermore, the MLPG can provide much better results in comparison with the finite element method at $\theta = \pm 60^{\circ}$.

**Example 6:**

This example is also that of an orthotropic cantilever beam with Young's moduli $E_1$ = 30, $E_2$ = 5, Poisson's ratios $\mu_{12}$ = 0·25 and the shear moduli $G_{12}$ = 2. The beam has the rectangular 'design domain' (L=2H) as shown in Fig. 15. The load P is applied at the middle of the right end.

The design domain is discretized using 40×20 uniformly distributed nodes. For the considered beam, optimized material directions (orientation angles) in minimum compliance design are shown in Fig.16.

Fig. 17 gives a comparison of the topology optimization results for isotropic and orthotropic material cantilever beam after the optimized orthotropic material directions are obtained.

**Example 7:**

Optimized material directions (orientation angles) in minimum compliance design of orthotropic MBB beam as in Fig.7 when using continuous angles as design variables. The problem is then solved using MLPG method. This MBB beam is discretized using 60 x 20 uniformly distributed nodes. The distribution of the optimized material directions is shown in fig.18 and topology optimization results in Fig.19.

Our displays of layouts for orthotropic planes reveal a very important effect of material directions for topology optimization results.

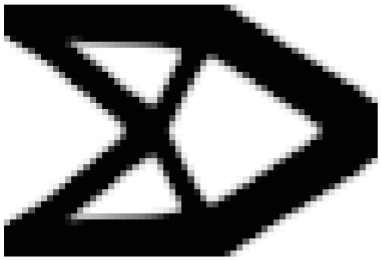

MLPG

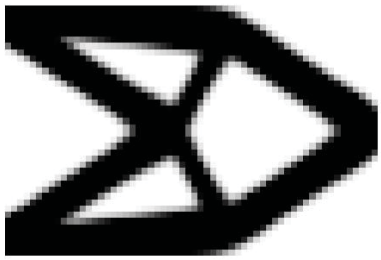

FEM

(a) Isotropic material

MLPG

FEM

(b) Orthotropic material (θ = -60°)

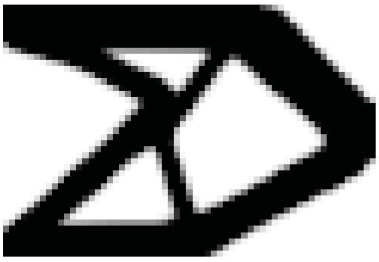

MLPG

FEM

(c) Orthotropic material (θ = 60°)

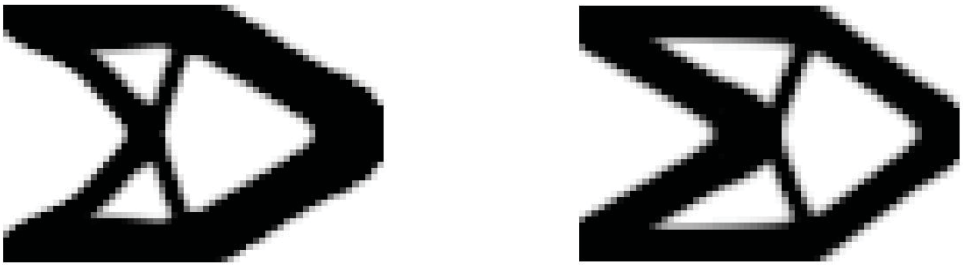

MLPG FEM

(d) Orthotropic material (θ = 90°)

MLPG FEM

(e) Orthotropic material (the optimized angle)

Figure 14: Comparison of topology optimization results

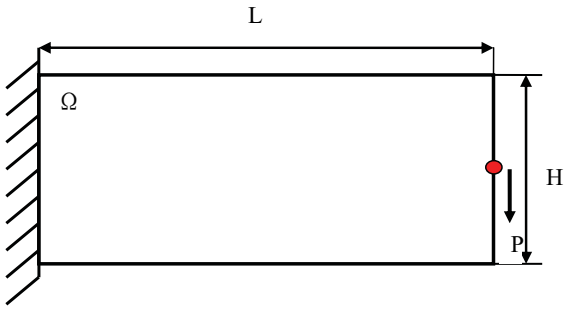


Figure 15: Cantilever beam (L=2H)

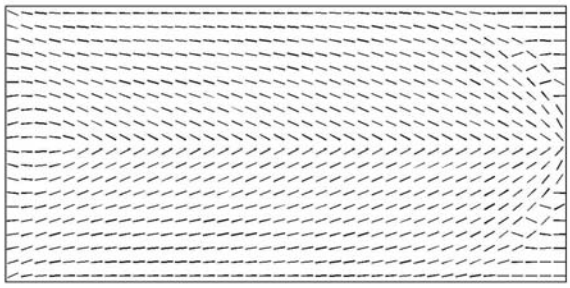

Figure 16: The distribution of orthotropic orientation

## 6 Conclusions

The structural design of an anisotropic solid involves an adaptation of the combined stages of the material-orientation optimization along with the topology optimization. Here we consider the optimization problem which minimizes the mean compliance of the structure. In the first stage, the material-orientation is the design variable without constraints (size optimization) and a sequential quadratic programming algorithm in which is a gradient based technique is used for efficient design. In the second stage, it is shown that different orientations of the same orthotropic material influence the optimal results of the global structure. The topology optimization problem is treated as the material distribution problem. The nodal values are used as the design variables, and the problem becomes one of finding the optimal values of the relative nodal volume fractions. In this paper, design domains are discretized by using the MLPG mixed collocation method, and a node with zero relative nodal volume fraction represents a void and a node with a relative nodal

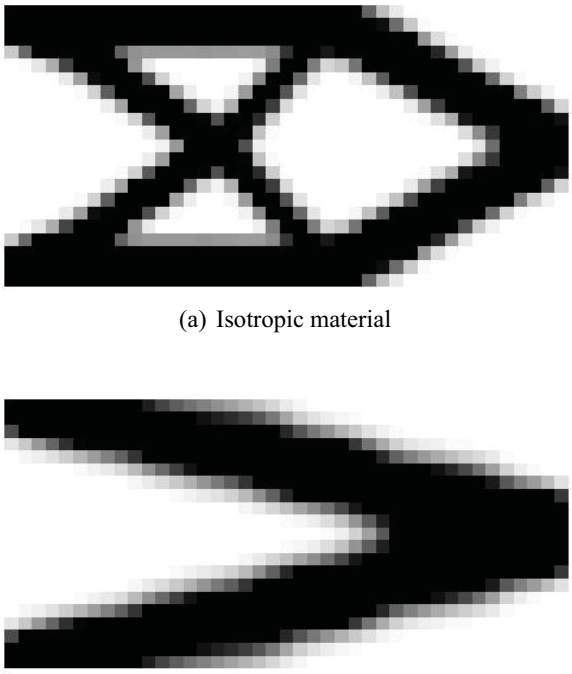

(a) Isotropic material

(b) Orthotropic material with the optimized orientation

Figure 17: Comparison of topology optimization results

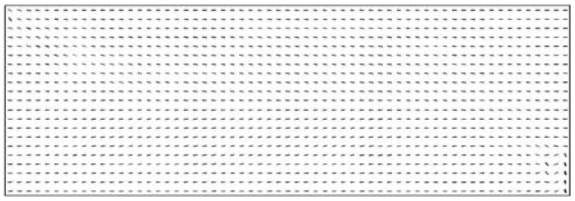

Figure 18: The distribution of orthotropic orientation

volume fraction of 1 represents a solid node. The goal is to find a distribution of relative nodal volume fractions that minimizes a compliance objective function, subject to volume constraints. To solve such a topology optimization problem, the popular optimality criteria (OC) based on the Lagrange method is employed with an iterative heuristic scheme for updating the design variables. In this paper, one of the significant findings is that of the topology optimized design for an orthotropic material results in a significantly different layout as compared to the isotropic material. This means that the solution space for the topology optimization problems is extended. So we

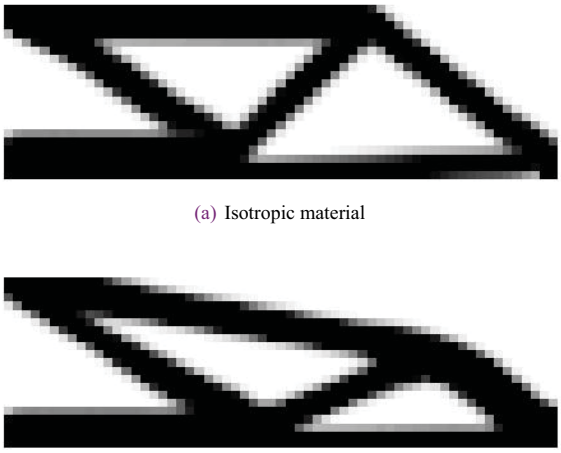

(a) Isotropic material

(b) Orthotropic material with the optimized orientation

Figure 19: Comparison of topology optimization results

have a considerably more flexible topology layout for an anisotropic solid, than when an isotropic material is used. The present method provides a physical insight into how the anisotropic material design variables interact to affect the topology properties of the structure.

We provide several numerical examples to demonstrate the versatility of the present method. For validation purposes, in some specific cases, the same topology optimization problem is solved using the finite element method, and the layouts can be compared with each other. The numerical instability problems related to a finite element mesh do not exist in the MLPG method. It need not cost extra CPU-time to deal with such numerical instabilities. The filtering technique is highly suitable for the present MLPG method.

**Acknowledgement:** This research was conducted during the study of Shu Li at UCI. The first author acknowledges the financial support of the National Natural Science Foundation of China (Grant No.10772013). This research was also partially supported by the Office of Naval Research and by the Office of the President of the University of California.

## References

**Atluri, S.N.; Zhu, T.** (1998): A New Meshless Local Petrov-Galerkin (MLPG) Approach in Computational Mechanics, *Computational Mechanics*, 22, 117-127.

**Atluri, S.N.; Shen, S.P.** (2002a): The meshless local Petrov-Galerkin (MLPG) method: A simple & less-costly alternative to the finite element and boundary element methods, *CMES: Computer Modeling in Engineering and Sciences,* 3 (1), 11-51.

**Atluri, S.N.; Shen, S.** (2002b): *The Meshless Local Petrov-Galerkin (MLPG) Method*, Tech Science Press.

**Atluri, S.N.** (2004): *The Meshless Method(MLPG) for Domain & BIE Discretizations*, Tech Science Press.

**Atluri, S.N.; Liu, H.T.; Han, Z.D.** (2006): Meshless local Petrov-Galerkin (MLPG) mixed collocation method for elasticity problems, *CMES: Computer Modeling in Engineering & Sciences*, 14 (3), 141-152.

**Bendsøe, M.P.; Kikuchi, N.** (1988): Generating optimal topologies in optimal design using a homogenization method, *Comp. Meth. Appl. Mech. Engrg.*, 71, 197-224.

**Cisilino, A.P.** (2006): Topology Optimization of 2D Potential Problems Using Boundary Elements, *CMES: Computer Modeling in Engineering & Sciences*, 15 (2), 99-106.

**Goh, C.J.; Yang, X.Q.** (2001): Nonlinear Lagrangian Theory for Nonconvex Optimization, *Journal of Optimization Theory and Applications*, 109 (1), 99-121.

**Khoshnood, A.; Jalali, M.A.** (2008): Normal oscillatory modes of rotating orthotropic disks, *Journal of Sound and Vibration,* 314, 147-160.

**Li, S.; Atluri, S.N.** (2008): Topology-optimization of structures based on the MLPG Mixed Collocation Method, *CMES: Computer Modeling in Engineering & Sciences*, 26 (1), 61-74.

**Norato, J.A.; Bendsøe, M.P.; Haber, R.B.; Tortorelli, D.A.** (2007): A topological derivative method for topology optimization, *Struct Multidisc Optim*, 33, 375-386.

**Pedersen, P.** (1989): On Optimal Orientation of Orthotropic Materials, *Struct. Optim.*, 1, 101-106.

**Sigmund, O.** (1994): Materials with prescribed constitutive parameters: An inverse homogenization problem, *Int. J. Solids Struct.*, 31, 2313-2329.

**Sigmund, O.** (1997): On the design of compliant mechanisms using topology optimization, *J. Mech. Struct. Mach.*, 25, 493-524.

**Sigmund, O.** (2001): A 99 line topology optimization code written in Matlab, *Struct Multidisc Optim.*, 21, 120-127.

**Spalatelu-Lazar, M.; Léné, F; Turbé, N.** (2008): Modelling and Optimization of Sails, *Computers and Structures*, 86, 1486-1493.

**Vemaganti, K.; Lawrence, W.E.** (2005): Parallel methods for optimality criteria-based topology optimization, *Comput. Methods Appl. Mech. Engrg.*, 194, 3637-3667.

**Wang, S.Y.; Lim, K.M.; Khoo, B.C.; Wang, M.Y.** (2007): A Geometric Deformation Constrained Level Set Method for Structural Shape and Topology Optimization, *CMES: Computer Modeling in Engineering & Sciences*, 18, (3), 155-181.

**Wang S.Y.; Lim K.M.; Khoo B.C.; Wang M.Y.** (2008): A Hybrid Sensitivity Filtering Method for Topology Optimization, *CMES: Computer Modeling in Engineering & Sciences*, 24 (1), 21-50.

**Zhou, S.; Wang, M.Y.** (2006): 3D Multi-Material Structural Topology Optimization with the Generalized Cahn-Hilliard Equations, *CMES: Computer Modeling in Engineering & Sciences*, 16 (2), 83-101.